

Myelination and long diffusion times alter diffusion-tensor-imaging contrast in myelin-deficient *shiverer* mice

Govind Nair,^a Yusuke Tanahashi,^{b,1} Hoi Pang Low,^b Susan Billings-Gagliardi,^c
William J. Schwartz,^b and Timothy Q. Duong^{d,*}

^aGraduate School of Biomedical Science, University of Massachusetts Medical School, Worcester MA 01655, USA

^bDepartment of Neurology, University of Massachusetts Medical School, Worcester MA 01655, USA

^cCell Biology, University of Massachusetts Medical School, Worcester MA 01655, USA

^dYerkes Research Center, Emory University, 954 N Gatewood Road, Atlanta, Georgia 30329, USA

Received 22 December 2004; revised 23 March 2005; accepted 20 May 2005

Available online 14 July 2005

Diffusion tensor imaging (DTI) using variable diffusion times (t_{diff}) was performed to investigate wild-type (wt) mice, myelin-deficient *shiverer* (*shi*) mutant mice and *shi* mice transplanted with wt neural precursor cells that differentiate and function as oligodendrocytes. At $t_{\text{diff}} = 30$ ms, the diffusion anisotropy “volume ratio” (VR), diffusion perpendicular to the fibers (λ_{\perp}), and mean apparent diffusion coefficient ($\langle D \rangle$) of the corpus callosum of *shi* mice were significantly higher than those of wt mice by $12 \pm 2\%$, $13 \pm 2\%$, and $10 \pm 1\%$, respectively; fractional anisotropy (FA) and relative anisotropy (RA) were lower by $10 \pm 1\%$ and $11 \pm 3\%$, respectively. Diffusion parallel to the fibers (λ_{\parallel}) was not statistically different between *shi* and wt mice. Normalized T_2 -weighted signal intensities showed obvious differences ($27 \pm 4\%$) between wt and *shi* mice in the corpus callosum but surprisingly did not detect transplant-derived myelination. In contrast, diffusion anisotropy maps detected transplant-derived myelination in the corpus callosum and its spatial distribution was consistent with the donor-derived myelination determined by immunohistochemical staining. Anisotropy indices (except λ_{\parallel}) in the corpus callosum showed strong t_{diff} dependence (30–280 ms), and the differences in λ_{\perp} and VR between wt and *shi* mice became significantly larger at longer t_{diff} s, indicative of improved DTI sensitivity at long t_{diff} . In contrast, anisotropy indices in the hippocampus showed very weak t_{diff} dependence and were not significantly different between wt and *shi* mice across different t_{diff} . This study provides insights into the biological signal sources and measurement parameters influencing DTI contrast, which could lead to developing more sensitive techniques for detection of demyelinating diseases.

© 2005 Elsevier Inc. All rights reserved.

Keywords: DTI; ADC; Diffusion anisotropy; MRI; High fields; Stem cell transplantation; Neural precursor cells; Myelin basic protein; Demyelination; STEAM sequence

Introduction

Diffusion tensor imaging (DTI) (Basser et al., 1994a,b) has gained wide acceptance as a tool for non-invasive imaging of anatomical connectivity (Mori, 1995; Nakada and Matsuzawa, 1995; Makris et al., 1997; Xue et al., 1999) and brain microstructural morphology (Mori et al., 2001a; Mori et al., 2001b; Zhang et al., 2002). DTI has been used for detecting changes in myelination in the developing brain (Wimberger et al., 1995; Prayer et al., 1997; Neil et al., 1998) and in demyelinating diseases (Guo et al., 2001; Larsson et al., 2004), although its underlying contrast mechanism remains incompletely understood. There is some evidence that DTI is more sensitive for detecting demyelinating lesions relative to conventional T_1 - and T_2 -weighted imaging (Hajnal et al., 1991; Sukama et al., 1991; Wimberger et al., 1995; Prayer et al., 1997; Guo et al., 2001; Larsson et al., 2004). DTI contrast arises from barriers (such as cell membranes of axons and oligodendrocytes) that hinder water diffusion in some orientations more than others, giving rise to anisotropic diffusion. In white matter of the central nervous system (CNS), for example, water diffusion perpendicular to fiber tracts is more restricted than that parallel to the fiber tracts (Le Bihan et al., 1993; Beaulieu and Allen, 1994b).

In principle, DTI contrast could arise from myelin and/or axons. Diffusion measurements on myelin-deficient and demyelinated fibers (Le Bihan et al., 1993; Beaulieu and Allen, 1994b; Ono et al., 1995; Seo et al., 1999; Gulani et al., 2001) showed that diffusion anisotropy was only marginally reduced relative to normal myelinated axonal fibers, suggesting that DTI contrast likely arises from axonal density and anisotropy in axonal structure rather than from myelin content. More recently, in vivo DTI study on dysmyelinated axons in myelin-deficient *shiverer* (*shi*) mutant mice (Song et al., 2002) reported small but significant reduction in diffusion anisotropy relative to wild-type (wt) mice, again suggesting that most of the DTI contrast arises from axons but myelin could contribute to DTI contrast. Although CNS axons in

* Corresponding author. Fax: +1 404 712 9917.

E-mail address: tduong@emory.edu (T.Q. Duong).

¹ Current address: Department of Physiology, Hokkaido University Graduate School of Medicine, Sapporo, Hokkaido, Japan.

Available online on ScienceDirect (www.sciencedirect.com).

shi mice remain apparently intact (Dupouey et al., 1979; Privat et al., 1979; Inoue et al., 1981; Shen et al., 1985), increased axonal protein content and abnormalities of the axonal cytoskeleton have been reported (Brady et al., 1999; Kirkpatrick et al., 2001). These and other potential pleiotropic effects associated with the *shi* mutation, which might modulate the apparent diffusion coefficient (ADC) and DTI contrast, remain to be addressed. Furthermore, the sensitivity of DTI contrast to detect changes in myelin per se has not been unequivocally demonstrated.

Most DTI studies use relatively short diffusion times (t_{diff}), typically ranging from 30 to 60 ms in animal model, in order to minimize signal loss due to T_2 decay. ADC has been shown to be t_{diff} -dependent (Segebarth et al., 1994; Helmer et al., 1995; Pfeuffer et al., 1998). ADC in the whole brain parenchyma had been reported to decrease rapidly from ~ 2 to ~ 15 ms and gradually decreases for $t_{\text{diff}} > 20$ ms (Segebarth et al., 1994; Helmer et al., 1995; Pfeuffer et al., 1998). The root-mean-squared (rms) displacement for $t_{\text{diff}} \sim 20$ ms approximates the ensemble-average distant between cell membranes (i.e., on the order of cell size). The effect of t_{diff} on DTI contrast at longer diffusion times (few hundreds of ms), however, remains relatively unexplored. Since diffusion displacement parallel to the fiber tracts in principle is less restricted, while that perpendicular to the fiber is more restricted, we predicted that DTI contrast should improve at longer t_{diff} . Knowledge of the t_{diff} -dependent effects on DTI contrast is important for future experiments aimed at improving sensitivity of fiber tracking.

The general aim of this study was to investigate the potential contribution of myelination and diffusion times to DTI contrast. First, we extended Song et al.'s (2002) study by systematically evaluating the sensitivity of diffusion perpendicular (λ_{\perp}) and parallel (λ_{\parallel}) to the fiber tracts, mean apparent diffusion coefficient ($\langle D \rangle$), fractional anisotropy (FA), relative anisotropy (RA), and volume ratio of the diffusion ellipsoid (VR) to detect anisotropy differences between wt and *shi* mice. Further, we performed the transplantation experiments to ask if and how MR parameters might be altered by the addition of some normal myelin to *shi* mice. We have previously shown that intracerebroventricular transplantation of neural precursor cells in *shi* mice leads to engraftment and differentiation of transplanted cells, including some that function as oligodendrocytes, producing wt myelin basic protein (MBP) and morphologically normal internodal myelin sheaths (Mitome et al., 2001). Such transplantation could potentially reverse the MRI abnormality observed in *shi* mice. DTI of wt, *shi*, and transplanted *shi* mice thus offered a unique opportunity to evaluate the effects of myelination per se on MR parameters. Second, we analyzed the sensitivity of DTI contrast as a function of t_{diff} (30 to 280 ms) in wt and *shi* mice. We modified the Stimulated-Echo-Acquisition-Mode (STEAM) sequence to include diffusion gradients, making it possible to use very long t_{diff} without substantial signal loss due to T_2 decay.

Materials and methods

Phantom experiments

Diffusion-weighted imaging (DWI) was performed using a modified STEAM sequence (Merboldt et al., 1991) with a pair of unipolar diffusion gradients placed during the TE/2 periods. The cross-term interactions of diffusion gradients with each other and with the imaging gradients might change the b values for different

diffusion-sensitive orientations (Brockstedt et al., 1998; Gullmar et al., 2002), possibly leading to bias in diffusion anisotropy within a single t_{diff} as well as across different t_{diff} . Although these gradient cross-term interactions could be calculated (Brockstedt et al., 1998; Gullmar et al., 2002), these calculations become tedious and inaccurate for STEAM sequence with very long diffusion time because the approximation used in the calculation may be invalid when the cross-terms are large. In this study, an experimental approach was used instead. This was done by experimentally adjusting the diffusion gradients (effective b values) such that the diffusion-weighted 1-D signal intensity profiles, and thus the diffusion coefficients, on a uniform water phantom along different diffusion-sensitizing directions were the same using identical imaging parameters as the in vivo part of this study. Phase-encoding gradients were switched off, and six profiles were obtained by sequentially switching on diffusion gradients in each of the six directions (3 axes, +1 and -1 direction for each axis). Since there were no first-order cross-terms in the phase-encoding direction, the profile intensities obtained with diffusion gradients in the phase-encoding directions were equal and these profiles were used as references. The magnitudes of the diffusion gradients in the slice-selection and readout directions were adjusted such that their profile intensities were equal to the reference profile intensities. Cross-terms from higher k -space lines were ignored because the positive and negative lobes of the phase-encoding gradients result in cancellation of the cross-term effects and the high k -space lines have relatively small "signal power". This correction was done for the larger (~ 1200 mm²/s) of the two b values; the cross-term effects on the low b value (~ 5 mm²/s) images were ignored. The advantage of this approach is that it can be readily validated experimentally across a wide range of conditions.

To test the validity of this approach, DTI measurements at different t_{diff} were made on a water phantom and a phantom of *N*-acetyl-aspartate (NAA) dissolved in dimethylsulfoxide (DMSO) at room temperature (20°C); the latter was chosen because it yielded a diffusion coefficient comparable to the ADC in the in vivo brain (i.e., gray matter) at 37°C.

Transplantation methods

Shi mice were used as transplantation hosts. The *shi* mutation is a large deletion in the MBP gene. Homozygous mutant mice fail to produce MBP, which is a major structural component of the myelin sheath, leading to extensive CNS dysmyelination with morphologically abnormal myelin sheaths. The *shi* mutation in our colony is maintained on a B6C3F1 hybrid-based stock, which is >99.9% congenic at other loci. Wide-type mice were obtained from the same hybrid stock.

Donor neural precursor cells were derived from the striatum/subventricular zone microdissected from embryonic transgenic mice on day 16 after overnight mating. These mice express an enhanced form of the jellyfish green fluorescent protein (GFP) under the control of the mouse prion promoter (Borchelt et al., 1996; van den Pol and Ghosh, 1998) and a chicken β -actin-cytomegalovirus immediate early enhancer (Niwa et al., 1991; Ikawa et al., 1995). Cells were isolated and propagated as previously described (Mitome et al., 2001). After 3–8 days in culture, these cells were harvested and transplanted into the brains of *shi* mice.

Neonatal *shi* host mice ranging in age from postnatal days 1 to 4 were cryoanesthetized and injected with 60,000 cells/1 μ l into each lateral cerebral ventricle, and 120,000 cells/2 μ l into the

cisterna magna. The cellular suspension was expelled gently via a glass micropipette that was inserted transcutaneously into the desired location with the aid of a stereotaxic apparatus.

Imaging was performed at 8–10 weeks old. After imaging, mice were deeply anesthetized with a solution of ketamine/xylazine and perfused with ice-cold heparinized phosphate-buffered saline, followed by ice-cold 4% buffered paraformaldehyde fixative. Brains were removed, tissues were fixed for 2–5 h at 4°C, and 50 μm thick coronal sections were cut on a vibratome and stored at -20°C in cryoprotectant. Free floating sections were processed for immunohistochemistry using a primary antibody directed against MBP (mouse, 1:1000 = 1 $\mu\text{g}/\text{ml}$; Sternberger Monoclonals, Lutherville, MD) and an anti-mouse Alexa Fluor 594 secondary antibody (Molecular Probes, Eugene, OR), as previously described (Mitome et al., 2001). Slides were examined using fluorescence microscopy, with excitation wavelengths for GFP and Alexa Fluor 594 of 488 and 568 nm, respectively.

MR imaging

Five groups of age-matched mice (8–10 weeks) were studied. T_2 -weighted imaging and DWI at short t_{diff} (= 30 ms) were performed on: (i) wt mice ($n = 7$), (ii) homozygous *shi* mice ($n = 8$), (iii) homozygous *shi* mice previously transplanted with neural precursor cells (transplant, $n = 6$). Of the 6 *shi* mice transplanted with precursor cells, 3 mice did not show significant GFP fluorescence post-mortem (failed transplant) and their MRI data were not further analyzed. Group iv consisted of homozygous *shi* mice previously transplanted with dead neural precursor cells which were killed by repeated freezing and thawing (Renfranz et al., 1991) (transplant control, $n = 3$). In Group v, multiple diffusion-time DTI experiments were performed on 5 wt mice and 5 *shi* mice from Groups i and ii.

Imaging was performed on spontaneously breathing mice under 1% isoflurane in air (~ 1 l/min). A custom-designed stereotaxic headset, consisting of ear bar, tooth bar, and shoulder bar, was used to immobilize the mouse head (Nair and Duong, 2004). Support was given to the legs and lower body with the mouse curved up slightly. Respiration rate, monitored with a force transducer and a differential amplifier and recorded onto an oscilloscope, was maintained within normal physiological ranges (120–150 bpm). Rectal temperature was maintained at $37.5 \pm 0.5^\circ\text{C}$ by circulating warm-water through a tube running underneath the mouse's body. Saline (0.3 ml, i.p.) was remotely administered via an extended PE-50 tubing every 2 h to prevent dehydration. Each mouse took ~ 5 h to image.

MRI was performed on a 9.4 T, 89 mm vertical magnet (Oxford Instruments, Oxford, UK) equipped with a Varian^{INOVA} console (Palo Alto, CA), a 100 Gauss/cm gradient (45 mm inner diameter and 100 μs rise time, Resonance Research Inc., Billerica, MA), and a custom-made surface coil (inner diameter = 1.5 cm). Six DWIs were acquired with $b = 1200$ s/mm^2 along 6 different oblique directions $\{(X,Y,0), (-X,Y,0), (X,0,Z), (-X,0,Z), (0,Y,Z), \text{and } (0,Y,-Z)\}$, and a seventh DWI was acquired with a low b value (5 s/mm^2) in the (X,Y,Z) direction (Basser and Pierpaoli, 1998). For the single short t_{diff} study, t_{diff} of 30 ms was used with mixing time $TM = 24$ ms, duration between diffusion gradient applications $\Delta = 31$ ms, and diffusion gradient duration $\delta = 3$ ms. For the multiple t_{diff} study, t_{diff} of 30, 80, 180, and 280 ms (acquisition order randomized) were achieved by modulating TM (and thus Δ). The shortest t_{diff} possible was 30 ms for the

conditions used herein. The other imaging parameters were repetition $TR = 2.5$ s, echo time $TE = 14$ ms, 4 averages, field of view (FOV) = 1.5 cm \times 1.5 cm, acquisition matrix = 64 \times 64, and seven 0.9-mm coronal slices with interslice spacing of 0.1 mm. T_2 -weighted images were also acquired using STEAM sequence with similar parameters as the low b value images at t_{diff} of 30 ms, but with a longer TE of 45 ms.

Data analysis

All data processing codes were written in Matlab® (Mathworks, Natick, MA) and displayed using STIMULATE software (University of Minnesota, MN). Acquisition matrix of 64 \times 64 was zero-filled to 128 \times 128 during reconstruction. ADC maps in 6 different directions were calculated. A 3 \times 3 diffusion tensor matrix (\mathbf{D}) was constructed and Eigenvalue decomposition was performed on the \mathbf{D} matrix to derive Eigenvalues λ_1 , λ_2 , and λ_3 and the corresponding Eigenvectors at each t_{diff} (Basser and Pierpaoli, 1998). $\langle D \rangle$, $\lambda_{//}$, λ_{\perp} , and anisotropy indices, namely: FA (range 0–1 with 0 being isotropic), RA (range 0– $\sqrt{2}$ with 0 being isotropic), and VR (range 0–1 with 1 being isotropic), were calculated using (Basser, 1995; Basser and Pierpaoli, 1998; Xue et al., 1999; Le Bihan et al., 2001):

$$\langle D \rangle = (\lambda_1 + \lambda_2 + \lambda_3)/3 \quad (1)$$

$$\lambda_{//} = \lambda_1; \text{ and } \lambda_{\perp} = (\lambda_2 + \lambda_3)/2 \quad \text{where } \lambda_1 \geq \lambda_2 \geq \lambda_3 \quad (2)$$

$$\text{FA} = \sqrt{3 \sum_{i=1}^3 (\lambda_i - \langle D \rangle)^2 / 2 \sum_{i=1}^3 \lambda_i^2} \quad (3)$$

$$\text{RA} = \sqrt{\sum_{i=1}^3 (\lambda_i - \langle D \rangle)^2 / 3 \langle D \rangle} \quad (4)$$

$$\text{VR} = \lambda_1 \times \lambda_2 \times \lambda_3 / \langle D \rangle^3 \quad (5)$$

FA color map was obtained by multiplying the FA index with the largest Eigenvector, and assigning three primary colors (red, green, and blue) to the three principal axes.

DTI parameters were analyzed using (1) region-of-interest (ROI) analysis and (2) spatial profile analysis. ROIs of the corpus callosum and hippocampus were drawn on the FA images (Fig. 4a) with reference to T_2 -weighted anatomical images. The corpus callosum was chosen as representative white matter because of its relatively large size and uniformity. Hippocampus was used as a control because it is largely composed of gray matter structures although there are some axons and white matter. The hippocampus was chosen retrospectively as it showed weak t_{diff} dependence. Cortex was not used because it has clear radially oriented structures. For demonstration, signal intensity spatial profile plots were projected along a line (4-pixel thick) crossing the corpus callosum in the ventral–dorsal direction at the level of the anterior commissure. For demonstration purpose, a single image slice that was similar across all animals was displayed for more accurate comparisons between different groups.

T_2 -weighted signal intensities in the corpus callosum were normalized with respect to the cortical gray matter within each animal for cross-subject comparison. The cortex was chosen over

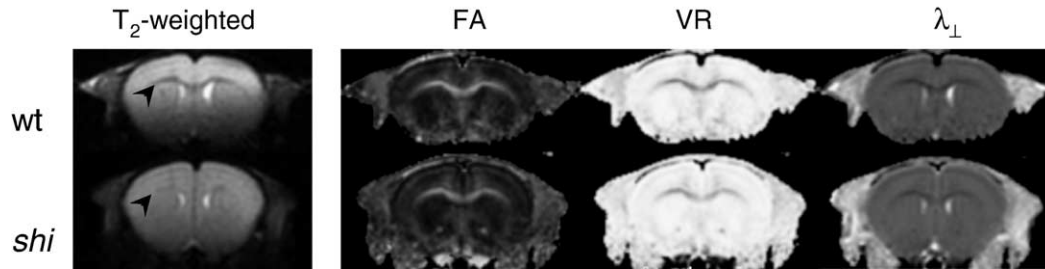


Fig. 1. Coronal T₂-weighted images, fractional anisotropy (FA), volume ratio (VR), diffusion perpendicular (λ_{\perp}) to the first Eigenvector obtained from a representative wild-type (wt), and a *shiverer* (*shi*) mouse brain at short (30 ms) diffusion time. T₂-weighted images show striking differences in the corpus callosum between wt and *shi* mice (arrowheads).

other possible structures because of its relatively uniform T₂ contrast and high signal-to-noise ratio. Comparison of T₂ maps would be ideal; unfortunately, the T₂ maps determined with two echo times and limited signal averaging herein were quite variable across animals and could not be used. Normalizing the T₂-weighted signal intensities with respect to the cortical gray matter within each animal made cross-subject comparison possible, although not ideal.

Statistical analysis used one-tail unpaired *t* test for comparing groups and mixed mode analysis for analyzing trends across t_{diff} . A *P* value <0.05 was considered to be statistically significant. Data in text are expressed as means \pm standard deviations.

Results

Phantom experiments

The adjustment factors for the diffusion gradients to minimize bias due to cross-term interactions were up to 7–14% for t_{diff} of 30 ms and 23–44% for 280 ms, with longer t_{diff} requiring larger corrections as expected. The surprisingly large correction factor was likely due to the very long diffusion time and the large diffusion gradients (~ 22 G/cm). Using the modified STEAM sequence with the experimental correction scheme, the measured water self-diffusion coefficients in a uniform phantom at 20°C ranged from 1.95×10^{-3} mm²/s to 2.0×10^{-3} mm²/s across different t_{diff} , consistent with those reported previously (Duong et al., 1998) albeit under slightly different temperatures. The measured diffusion coefficient of NAA in DMSO from a uniform spherical phantom at 20°C ranged from 0.50×10^{-3} to 0.52×10^{-3} mm²/s across different diffusion directions and t_{diff} . No published literature data were found for comparison. Diffusion coefficients and DTI parameters (λ_{\perp} , λ_{\parallel} , $\langle D \rangle$, FA, RA, and VR) in the uniform phantoms were not statistically different across different diffusion directions or across different t_{diff} .

Table 1

Group-average normalized T₂-weighted signal intensities, fractional anisotropy (FA), volume ratio (VR), water diffusion perpendicular to (λ_{\perp}) and parallel to (λ_{\parallel}) the direction of the axonal fibers, relative anisotropy (RA), and mean apparent diffusion coefficient ($\langle D \rangle$) obtained from the corpus callosum of wild-type (wt, $n = 7$) and *shiverer* (*shi*, $n = 8$) mice at 30 ms diffusion time

	T ₂ -weighted (normalized)	FA	VR	λ_{\perp} ($\times 10^{-3}$ mm ² /s)	λ_{\parallel} ($\times 10^{-3}$ mm ² /s)	RA	$\langle D \rangle$ ($\times 10^{-3}$ mm ² /s)
wt	0.77 \pm 0.04	0.52 \pm 0.02	0.69 \pm 0.04	0.48 \pm 0.02	1.16 \pm 0.09	0.27 \pm 0.02	0.70 \pm 0.03
<i>shi</i>	0.98 \pm 0.04	0.47 \pm 0.02	0.77 \pm 0.03	0.54 \pm 0.02	1.21 \pm 0.07	0.24 \pm 0.02	0.77 \pm 0.03
% changes	27 \pm 4	-10 \pm 1	12 \pm 2	13 \pm 2	4 \pm 1	-11 \pm 3	10 \pm 1
<i>P</i> value	<10 ⁻⁴	<10 ⁻³	$\sim 10^{-2}$	<10 ⁻⁴	0.33	0.01	0.01

The ROIs used were similar to that of Fig. 4a. *P* values (one-tail unpaired *t* test) indicate statistical significances between wt and *shi* mice.

DTI of wt and *shi* mice

Fig. 1 shows representative T₂-weighted images, FA, VR, and λ_{\perp} maps from a wt and a *shi* mouse. T₂-weighted images showed dramatic differences in the pixel intensity of the corpus callosum (arrowheads) between wt and *shi* mice whereas FA, VR, and λ_{\perp} maps showed only subtle differences. The group-average FA, VR, λ_{\perp} , λ_{\parallel} , and $\langle D \rangle$ from corpus callosum (Fig. 4a) were quantified and are summarized in Table 1. The group-average normalized T₂-weighted signal intensities, VR, λ_{\perp} , and $\langle D \rangle$ from the corpus callosum of *shi* mice were significantly higher than those of wt mice ($P < 0.05$); FA and RA of *shi* mice were significantly lower than those of wt mice ($P < 0.05$). λ_{\parallel} was, however, not statistically different in wt and *shi* mice ($P < 0.05$). The magnitude differences and statistical significances between wt and *shi* groups were highest in VR followed by FA and smallest in RA, although the percentage changes were similar.

To graphically demonstrate the differences between wt and *shi* mice, spatial profiles of the normalized T₂-weighted signal intensities of wt and “*shi* + transplant control” groups were plotted starting at the caudate putamen, crossing the corpus callosum, to the cortical gray matter (Fig. 2a). It should be noted that the spatial profiles of the *shi* and the transplant control groups were not statistically different from each other and were therefore grouped together as “*shi* + transplant control” as shown. Normalized T₂-weighted signal intensities in wt and “*shi* + transplant control” groups were similar in the gray matter but were markedly different in the corpus callosum. Likewise, spatial profiles of FA maps (Fig. 2b) from wt and “*shi* + transplant control” groups were similar in the gray matter but differed significantly in the corpus callosum.

Effects of precursor cell transplantation on DTI contrast

To investigate the signal sources leading to different DTI contrast between wt and *shi* mice, DTI was performed on *shi* mice

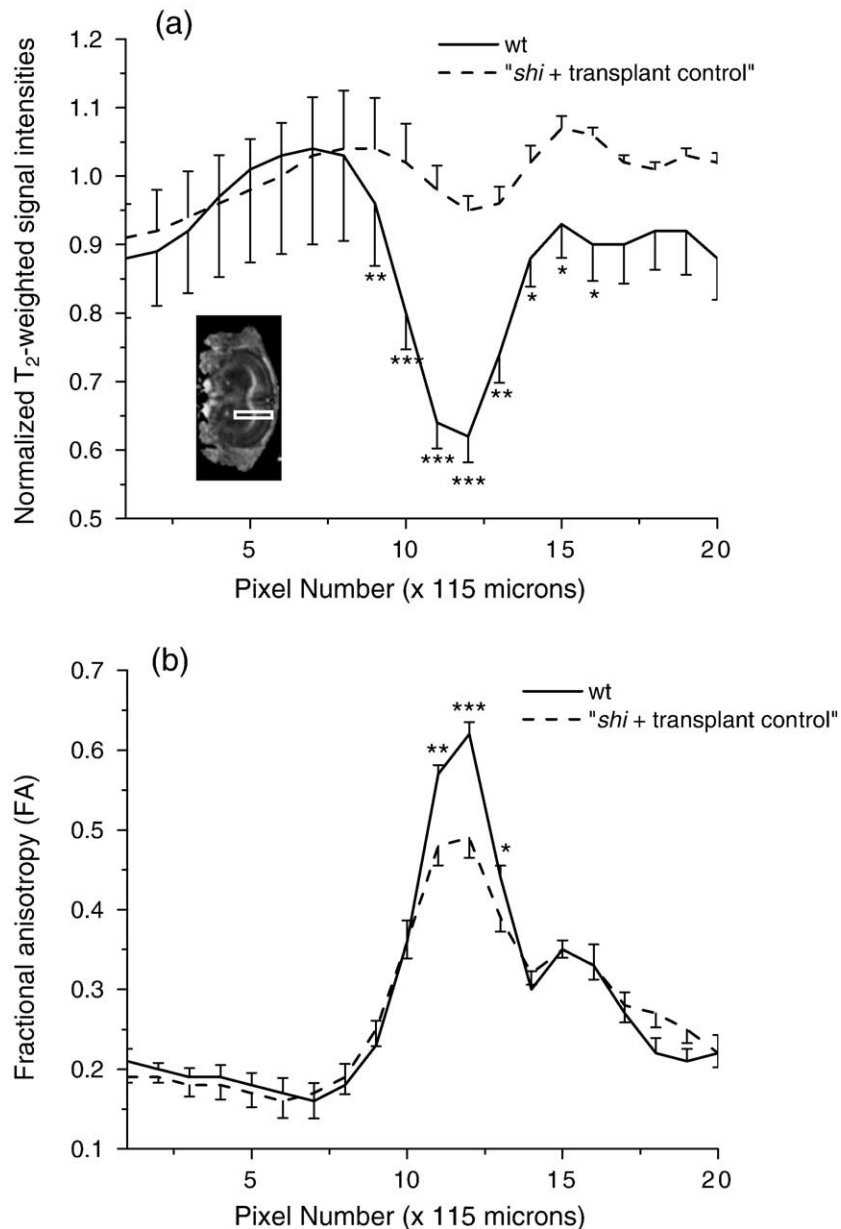


Fig. 2. Group-average spatial profiles of (a) T_2 -weighted signal intensity normalized to cortical gray matter and (b) fractional anisotropy (FA) obtained crossing the corpus callosum of the wt (mean \pm SEM, $n = 7$) and “*shi* + transplant control” (mean \pm SEM, $n = 8$ for *shi*, and $n = 3$ for transplant control). The spatial profile starts at gray matter in the caudate putamen, crosses the corpus callosum, and ends with gray matter in the cortex, as shown in the inset. * $P < 0.05$, ** $P < 0.01$, *** $P < 0.001$.

transplanted with myelin-producing wt neural precursor cells. The group-average FA value of the corpus callosum in the transplanted mice was found to be intermediate between those of wt and “*shi* + transplant control” mice (Fig. 3a) but was highly variable. On the contrary and surprisingly, the group-average normalized T_2 -weighted intensity spatial profile of the transplanted mice was similar to that of the “*shi* + transplant control” mice (data not shown).

For detailed investigation, results from two individual animals are discussed below. Transplanted mouse #2 showed essentially normal values of FA in the corpus callosum, consistent with the highest density of donor-derived wt MBP immunoreactivity and GFP cellular distribution observed among the transplanted animals

studied (Fig. 3b). However, normalized T_2 -weighted signal intensities in the corpus callosum did not show recovery; rather, they appeared similar to that of the “*shi* + transplant control” group (Fig. 3b).

Another transplanted mouse (#5) showed grossly asymmetric hemispheric GFP cellular distribution and wt MBP immunoreactivity in the corpus callosum, although neural precursor cells had been injected in both cerebral lateral ventricles and cisterna magna. FA image in grayscale appeared brighter in the corpus callosum of the hemisphere with relatively more successful transplantation (Fig. 3c). FA color tensor map did not show any apparent abnormality in the directionality of the white matter fibers of the donor-derived myelin.

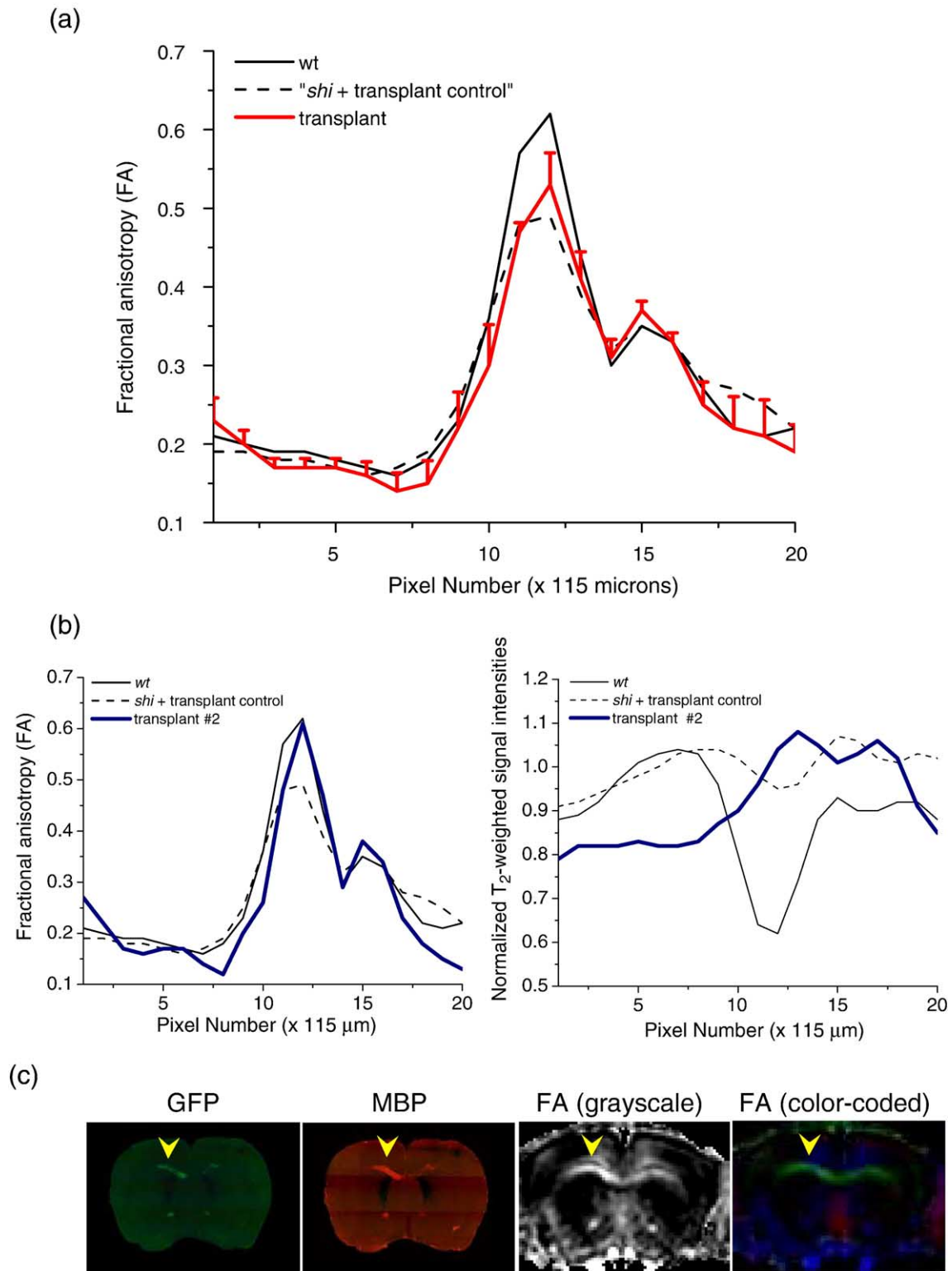


Fig. 3. (a) Spatial profile plot of fractional anisotropy (FA) obtained crossing the corpus callosum of the transplanted mice ($n = 3$, mean \pm SEM). Group-average data of wt and “*shi* + transplant control” groups are re-plotted without error bars from Fig. 2 for comparison. (b) Spatial profile plots of FA and normalized T_2 -weighted signal intensities of transplant mouse #2. Group-average data of the wt and “*shi* + transplant control” group are re-plotted without error bars from Fig. 2 for comparison. The peak at pixel # 15 arises from a white matter track projecting into the cortex and is not an artifact. (c) Histological sections showing locations of donor-derived green fluorescent protein (GFP) cells and myelin basic protein (MBP) immunoreactivity and the corresponding grayscale FA map and color-coded directional FA map from transplanted mouse #5. Donor-derived myelination by the transplanted precursor cells in the corpus callosum showed asymmetric distribution between the two hemispheres corresponding to FA maps (arrowheads).

DTI contrast at variable t_{diff}

Sensitivity of DTI parameters to different t_{diff} was evaluated for the corpus callosum and the hippocampal gray matter in wt and *shi*

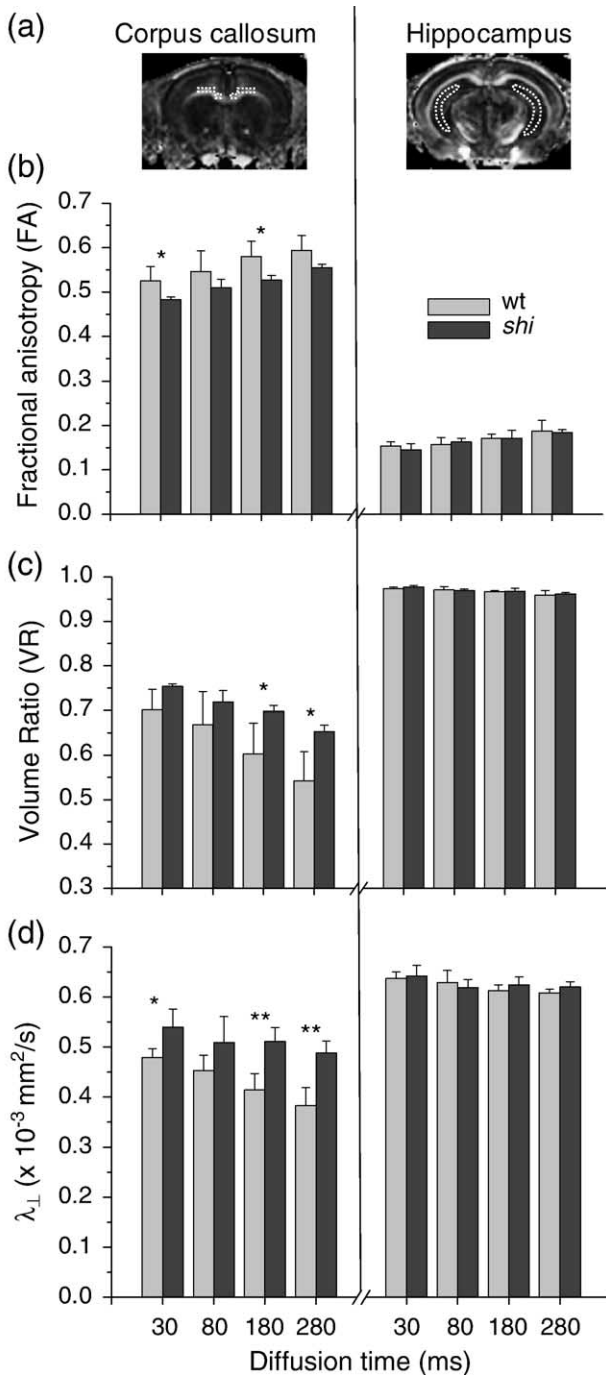


Fig. 4. (a) Representative ROIs of the corpus callosum and the hippocampus overlaid on fractional anisotropy (FA) maps. Group-average (b) FA, (c) volume ratio (VR), and (d) diffusion perpendicular to the first Eigenvector (λ_{\perp}) of the corpus callosum and hippocampus from wt and *shi* mice at different diffusion times. FA, VR, and λ_{\perp} of the corpus callosum show significantly stronger t_{diff} dependent relative to those of the hippocampus. Differences in VR and λ_{\perp} between wt and *shi* mice became significantly larger at longer t_{diff} in the corpus callosum. Values in plot are mean \pm SD for $n = 5$. * $P < 0.05$, ** $P < 0.01$.

mice. Representative ROIs used in the analysis are shown in Fig. 4a. There was a strong trend toward increasing diffusion anisotropy with increasing t_{diff} ($P < 0.05$). The group-average FA (Fig. 4b), VR (Fig. 4c), and λ_{\perp} (Fig. 4d) show increasing significant differences in λ_{\perp} and VR between wt and *shi* mice at longer t_{diff} ($P < 0.05$). λ_{\parallel} was, however, not statistically different in wt and *shi* mice ($P > 0.05$, data not shown).

By contrast, the dependence of anisotropy indices on t_{diff} in the hippocampus was significantly less pronounced compared to that in the corpus callosum. The group-average FA (Fig. 4b), VR (Fig. 4c), λ_{\perp} (Fig. 4d), and λ_{\parallel} in the hippocampus were not statistically different between wt and *shi* mice at all t_{diff} ($P > 0.05$).

Discussion

The major findings of this study are: (1) T₂-weighted images detected obvious differences between wt and *shi* mice in the corpus callosum but surprisingly did not detect donor-derived myelination in *shi* mice transplanted with neural precursor cells. By contrast, FA showed comparatively smaller differences between wt and *shi* mice in the corpus callosum but detected changes due to donor-derived myelination in the transplant group. Despite the presence of partial-volume effect from limited spatial resolution, various analysis approaches yielded consistent results and interpretation across different DTI parameters. (2) A modified STEAM sequence with an experimental cross-term correction scheme was implemented. In contrast to those in the hippocampus, DTI parameters in the corpus callosum showed markedly stronger t_{diff} dependence, and the differences in these parameters between wt and *shi* mice grew larger at longer t_{diff} , indicative of improved DTI sensitivity at longer t_{diff} .

DTI of wt, *shi*, and transplanted mice at short t_{diff}

Differences in λ_{\perp} and RA between *shi* and wt mice in vivo have been previously reported, with λ_{\perp} being more sensitive and yielded more consistent changes than RA (Song et al., 2002). Our findings are in agreement with those of Song et al. (2002). Furthermore, we compared the sensitivity of RA, FA, and VR to detect differences in myelination between wt and *shi* mice and found that RA was the least sensitive of the three anisotropy indices, likely due to the small dynamic range for the typical RA values in vivo (Ulug and van Zijl, 1999; Partridge et al., 2004). This notion was consistent with our simulation study in which different RA, FA, and VR were calculated over the biologically relevant ranges based on experimentally measured λ_{\perp} and λ_{\parallel} (data not shown). VR shows the largest dynamic range likely because the actual Eigenvalues, rather than variances of the Eigenvalues (as in FA or RA), were used in the definition. The sensitivity of RA was further reduced because $\langle D \rangle$ was used as the normalization factor (as opposed to the actual Eigenvalues used in the FA calculation).

In addition, we also performed transplantation of wt neural precursor cells to address the potential pleiotropic effects associated with the *shi* mutation. The contribution of myelin per se on DTI parameters could thus be directly evaluated. DTI parameters of animals with successful transplantation of neural precursor cell clearly demonstrated that the measured DTI parameters became closer to that of wt, although the sample size was small due to the challenging transplantation experiments. Further, regions with

increased diffusion anisotropy showed good correspondence to the spatial distributions of donor-derived myelination in individual mouse brains as indicated by MBP immunohistochemistry and GFP cellular distribution.

One surprising finding is that although T_2 -weighted images yielded dramatic differences between wt and *shi* mice in the corpus callosum, T_2 -weighted images and semi-quantitative normalized T_2 -weighted signals did not appear to be sensitive to transplant-derived myelination. Although the sensitivity of T_2 to detect changes in myelin has been an issue of debate, myelin content had been reported to correlate with T_2 (MacKay et al., 1994; Stanisz et al., 2004). We have no definitive explanation for this apparent discrepancy. One potential explanation for the lack of observable T_2 changes in transplanted *shi* mice is that normal and densely packed myelin might be necessary for T_2 contrast (Fig. 1), whereas a partial recovery might be sufficient to induce an observable DTI contrast in white matter. While further validation is needed, our results are consistent with those reported by Guo et al. (2001), who found RA to be more sensitive than T_2 -weighted images in detecting dysmyelination in human Krabbe's disease and stem-cell transplantation. Similarly, Larsson et al. (2004) found that DTI is relatively more sensitive than T_1 - or T_2 -weighted images in delineating myelin-related lesions.

As mentioned above, although CNS axons in *shi* mice remain apparently intact (Dupouey et al., 1979; Privat et al., 1979; Inoue et al., 1981; Shen et al., 1985), increased axonal protein content and abnormalities of the axonal cytoskeleton have been reported (Brady et al., 1999; Kirkpatrick et al., 2001). Transplant control experiments argue against the possibility that MR effects might be due to the surgical procedure per se. The combined "transplant" and "transplant control" experiments thus allowed us to cautiously conclude that the observed changes in DTI parameters indeed indicate changes due to myelin. Nonetheless, the transplanted myelin could, in principle, prevent some axonal loss in *shi* mice, and thus the notion that "axonal loss" resulted in the observed changes in DTI parameters could not be completely excluded. Relating particular changes in the MR parameters to the specific tissue pathology is evidently challenging because diseases are complex and many tissue pathologies result in similar changes of MR parameters.

Technical considerations for the variable t_{diff} experiments

Diffusion measurements at long t_{diff} using spin-echo sequences are not common because of the short T_2 of brain tissue water (i.e., gray matter $T_2 \sim 40$ ms at 9.4 T). The modified STEAM sequence allows diffusion measurements to be performed at very long t_{diff} (Merboldt et al., 1991; Horsfield et al., 1994) because the t_{diff} is placed during the TM period where the signal loss due to T_1 recovery, as opposed to T_2 decay, is relatively small (gray matter $T_1 \sim 1.9$ s at 9.4 T). The drawback of the STEAM sequence is that the stimulated-echo acquisition retains only half of the magnetization and thus the signal-to-noise ratio (SNR) is reduced by half. Reduction in SNR was, however, partially compensated by using a relatively short echo time (14 ms), high magnetic field, and a small surface coil.

Varying t_{diff} by changing TM in the STEAM sequence could result in reduced SNR at longer t_{diff} and preferential weighting toward water molecules with long T_1 , which could confound the interpretation of the t_{diff} -dependent effect. Although not negligible, SNR reduction with increasing t_{diff} was relatively small due to the

long T_1 and high SNR at high field. Reduced SNR could be compensated by increasing signal averaging at long t_{diff} . Increased anisotropy observed with increasing t_{diff} could in principle be due to T_1 weighting of white matter at the expense of gray matter within a voxel (partial volume effect). However, white matter, which has shorter T_1 than gray matter, is expected to be weighted less in the STEAM sequence. Thus, the T_1 effect could not explain the observed t_{diff} -dependent effects, and the reported t_{diff} dependence was likely a conservative estimate.

Finally, SNR could potentially affect diffusion anisotropy. As the SNR of the DWI decreases, the apparent diffusion anisotropy calculated from the tensors tends to increase due to a statistical biasing effect (Pierpaoli and Basser, 1996; Basser and Pierpaoli, 1998). Thus, it is possible that the trend of increasing diffusion anisotropy with increasing t_{diff} is artificial. Against this possibility is our observation that control hippocampus data did not show such trend. Thus, the increasing diffusion anisotropy of the corpus callosum with increasing t_{diff} could not be artificial.

Improved DTI sensitivity at long t_{diff}

In the presence of restricted and anisotropic diffusion, a longer t_{diff} (Segebarth et al., 1994; Helmer et al., 1995; Pfeuffer et al., 1998) could in principle improve DTI contrast. However, such effect has not been systematically investigated. Although the biological system is considerably more complex, restricted diffusion in vivo could be hypothetically categorized into two regimes, one where the root-mean-squared (rms) displacement is on the orders of the average cell size and the other where the rms displacement is significantly larger than the average cell size. ADC measurements on ex vitro large squid axons showed that at very short t_{diff} of ~ 2 ms, the ADC perpendicular to the axonal fibers was high and close to the ADC parallel to the axonal fibers. When t_{diff} was lengthened to 28 ms, the ADC perpendicular to the axonal fibers was reduced by half, whereas ADC parallel to the axonal fibers was largely unchanged (Beaulieu and Allen, 1994a). Similarly, significant reduction in λ_{\perp} for t_{diff} ranging from 5 to 50 ms had been reported using multiple quantum experiments (Seo et al., 1999).

At the other regime where the rms displacement is significantly larger than the average cell size, restricted diffusion arises predominantly with extracellular diffusion and the t_{diff} is on the orders of tens to hundreds of milliseconds. Such restricted diffusion has been previously reported. White matter ADC (not DTI) in the human brain showed a t_{diff} dependence for t_{diff} ranging from 40 to 800 ms (Horsfield et al., 1994) although these data were obtained with variable b values which yielded differential weighting to different spin populations and confounded interpretation of the t_{diff} -dependent effects. In our study, we investigated DTI contrast at long t_{diff} (30 to 280 ms) and found strong t_{diff} dependence in the corpus callosum. DTI at all t_{diff} was measured in each animal and pair-wise comparison within the same animals made the trend relatively more apparent. In contrast, Le Bihan reported that non-significant changes in ADC perpendicular and parallel to the fiber tracts in humans were observed for t_{diff} ranging from 16 to 79 ms (Le Bihan et al., 1993). Indeed, our data showed small and non-significant differences in DTI parameters between t_{diff} of 30 ms and 80 ms for both wt and *shi* mice. In short, these results suggest improvement in DTI contrast at long t_{diff} . The biophysical mechanism(s) underlying the t_{diff} -dependent DTI contrast and diffusion restriction across these long diffusion times, however, remains to be elucidated.

Conclusions

This study provided a better understanding of the signal sources and measurement parameters underlying DTI contrasts. This could lead to developing more sensitive techniques for detection and monitoring of progression and therapeutic intervention of demyelinating diseases.

Acknowledgments

The authors would like to acknowledge Drs. Susumu Mori and Hangyi Jiang of Johns Hopkins University for their help during the development of our DTI processing codes, Dr. Karl G. Helmer of Worcester Polytechnic Institute and Dr. Qin Liu of University of Massachusetts Medical School for technical advice and assistance. This work was supported in part by the Whitaker Foundation (RG-02-0005), the American Heart Association (SDG-0430020N) to TQD, NASA grant NAG9-1356 to WJS, and the NIH/NCRR base grant to the “Yerkes National Primate Research Center, Emory University,” (RR-00165).

References

- Basser, P.J., 1995. Inferring microstructural features and the physiological state of tissues from diffusion-weighted images. *NMR Biomed.* 8, 333–344.
- Basser, J.P., Pierpaoli, C., 1998. A simplified method to measure the diffusion tensor from seven MR images. *Magn. Reson. Med.* 39, 928–934.
- Basser, P.J., Mattiello, J., LeBihan, D., 1994a. Estimation of the effective self-diffusion tensor from the NMR spin echo. *J. Magn. Reson., B* 103, 247–254.
- Basser, P.J., Mattiello, J., LeBihan, D., 1994b. MR diffusion tensor spectroscopy and imaging. *Biophys. J.* 66, 259–267.
- Beaulieu, C., Allen, P.S., 1994a. Water diffusion in the giant axon of the squid: implications for diffusion-weighted MRI of the nervous system. *Magn. Reson. Med.* 32, 579–583.
- Beaulieu, C., Allen, P.S., 1994b. Determinants of anisotropic water diffusion in nerves. *Magn. Reson. Med.* 31, 394–400.
- Borchelt, D.R., Davis, J., Fischer, M., Lee, M.K., Slunt, H.H., Ratovitsky, T., Regard, J., Copeland, N.G., Jenkins, N.A., Sisodia, S.S., Price, D.L., 1996. A vector for expressing foreign genes in the brains and hearts of transgenic mice. *Genet. Anal.* 13, 159–163.
- Brady, S.T., Witt, A.S., Kirkpatrick, L.L., de Waegh, S.M., Readhead, C., Tu, P.H., Lee, V.M., 1999. Formation of compact myelin is required for maturation of the axonal cytoskeleton. *J. Neurosci.* 19, 7278–7288.
- Brockstedt, S., Thomsen, C., Wirestam, R., Holtas, S., Stahlberg, F., 1998. Quantitative diffusion coefficient maps using fast spin-echo MRI. *Magn. Reson. Imaging* 16, 877–886.
- Duong, T.Q., Ackerman, J.J.H., Ying, H.S., Neil, J.J., 1998. Evaluation of extra- and intracellular apparent diffusion in normal and globally ischemic rat brain via 19 F NMR. *Magn. Reson. Med.* 40, 1–13.
- Dupouey, P., Jacque, C., Bourre, J.M., Cesselin, F., Privat, A., Baumann, N., 1979. Immunochemical studies of myelin basic protein in shiverer mouse devoid of major dense line of myelin. *Neurosci. Lett.* 12, 113–118.
- Gulani, V., Webb, A.G., Duncan, I.D., Lauterbur, P.C., 2001. Apparent diffusion tensor measurements in myelin-deficient rat spinal cords. *Magn. Reson. Med.* 45, 191–195.
- Gullmar, D., Jaap, T., Bellemann, M.E., Hauelsen, J., Reichenbach, J.R., 2002. DTI measurements of isotropic and anisotropic media. *Biomed. Tech. (Berl)* 47, 420–422.
- Guo, A.C., Petrella, J.R., Kurtzberg, J., Provenzale, J.M., 2001. Evaluation of white matter anisotropy in Krabbe disease with diffusion tensor MR imaging: initial experience. *Radiology* 218, 809–815.
- Hajnal, J.V., Doran, M., Hall, A.S., Collins, A.G., Oatridge, A., Pennock, J.M., Young, I.R., Bydder, G.M., 1991. MR imaging of anisotropically restricted diffusion of water in the nervous system: technical, anatomic, and pathologic considerations. *J. Comput. Assist. Tomogr.* 15, 1–18.
- Helmer, K.G., Dardzinski, B.J., Sotak, C.H., 1995. The application of porous-media theory to the investigation of time-dependent diffusion in vivo systems. *NMR Biomed.* 8, 297–306.
- Horsfield, M.A., Barker, G.J., McDonald, W.I., 1994. Self-diffusion in CNS tissue by volume-selective proton NMR. *Magn. Reson. Med.* 31, 637–644.
- Ikawa, M., Kominami, K., Yoshimura, Y., Tanaka, K., Nishimune, Y., Okabe, M., 1995. A rapid and non-invasive selection of transgenic embryos before implantation using green fluorescent protein (GFP). *FEBS Lett.* 375, 125–128.
- Inoue, Y., Nakamura, R., Mikoshiba, K., Tsukada, Y., 1981. Fine structure of the central myelin sheath in the myelin deficient mutant shiverer mouse, with special reference to the pattern of myelin formation by oligodendroglia. *Brain Res.* 219, 85–94.
- Kirkpatrick, L.L., Witt, A.S., Payne, H.R., Shine, H.D., Brady, S.T., 2001. Changes in microtubule stability and density in myelin-deficient shiverer mouse CNS axons. *J. Neurosci.* 21, 2288–2297.
- Larsson, E.M., Englund, E., Sjobeck, M., Latt, J., Brockstedt, S., 2004. MRI with diffusion tensor imaging post-mortem at 3.0 T in a patient with frontotemporal dementia. *Dementia Geriatr. Cognit. Disord.* 17, 316–319.
- Le Bihan, D., Turner, R., Douek, P., 1993. Is water diffusion restricted in human brain white matter? An echo-planar NMR imaging study. *NeuroReport* 4, 887–890.
- Le Bihan, D., Mangin, J.F., Poupon, C., Clark, C.A., Pappata, S., Molko, N., Chabriat, H., 2001. Diffusion tensor imaging: concepts and applications. *J. Magn. Reson. Imaging* 13, 534–546.
- MacKay, A., Whittall, K., Adler, J., Li, D., Paty, D., Graeb, D., 1994. In vivo visualization of myelin water in brain by magnetic resonance. *Magn. Reson. Med.* 31, 673–677.
- Makris, N., Worth, A.J., Sorensen, A.G., Papadimitriou, G.M., Wu, O., Reese, T.G., Wedeen, V.J., Davis, T.L., Stakes, J.W., Caviness, V.S., Kaplan, E., Rosen, B.R., Pandya, D.N., Kennedy, D.N., 1997. Morphometry of in vivo human white matter association pathways with diffusion-weighted magnetic resonance imaging. *Ann. Neurol.* 42, 951–962.
- Merboldt, K.D., Hanicke, W., Frahm, J., 1991. Diffusion imaging using stimulated echoes. *Magn. Reson. Med.* 19, 233–239.
- Mitome, M., Low, H.P., van den Pol, A., Nunnari, J.J., Wolf, M.K., Billings-Gagliardi, S., Schwartz, W.J., 2001. Towards the reconstruction of central nervous system white matter using neural precursor cells. *Brain* 124, 2147–2161.
- Mori, K., 1995. Relation of chemical structure to specificity of response in olfactory glomeruli. *Curr. Opin. Neurobiol.* 5, 467–474.
- Mori, S., Itoh, R., Kaufmann, W.E., van Zijl, P.C.M., Solaiyappan, M., Yarowsky, P., 2001a. Diffusion tensor imaging of the developing mouse brain. *Magn. Reson. Med.* 46, 18–23.
- Mori, S., Itoh, R., Zhang, J., Kaufmann, W.E., van Zijl, P.C., Solaiyappan, M., Yarowsky, P., 2001b. Diffusion tensor imaging of the developing mouse brain. *Magn. Reson. Med.* 46, 18–23.
- Nair, G., Duong, T.Q., 2004. Echo-planar BOLD fMRI of mice on a narrow-bore 9.4 T magnet. *Magn. Reson. Med.* 52, 430–434.
- Nakada, T., Matsuzawa, H., 1995. Three-dimensional anisotropy contrast magnetic resonance imaging of the rat nervous system: MR axonography. *Neurosci. Res.* 22, 389–398.
- Neil, J.J., Shiran, S.I., McKinstry, R.C., Scheff, G.L., Snyder, A.Z., Almlí, C.R., Akbudak, E., Aronovitz, J.A., Miller, J.P., Lee, B.C., Conturo, T.E., 1998. Normal brain in human newborns: apparent diffusion coefficient and diffusion anisotropy measured by using diffusion tensor MR imaging. *Radiology* 209, 57–66.

- Niwa, H., Yamamura, K., Miyazaki, J., 1991. Efficient selection for high-expression transfectants with a novel eukaryotic vector. *Gene* 108, 193–199.
- Ono, J., Harada, K., Takahashi, M., Maeda, M., Ikenaka, K., Sakurai, K., Sakai, N., Kagawa, T., Fritz-Zieroth, B., Nagai, T., et al., 1995. Differentiation between dysmyelination and demyelination using magnetic resonance diffusional anisotropy. *Brain Res.* 671, 141–148.
- Partridge, S.C., Mukherjee, P., Henry, R.G., Miller, S.P., Berman, J.I., Jin, H., Lu, Y., Glenn, O.A., Ferriero, D.M., Barkovich, A.J., Vigneron, D.B., 2004. Diffusion tensor imaging: serial quantitation of white matter tract maturity in premature newborns. *Neuroimage* 22, 1302–1314.
- Pfeuffer, J., Fogel, U., Dreher, W., Leibfritz, D., 1998. Restricted diffusion and exchange of intracellular water: theoretical modelling and diffusion time dependence of ^1H NMR measurements on perfused glial cells. *NMR Biomed.* 11, 19–31.
- Pierpaoli, C., Basser, P.J., 1996. Toward a quantitative assessment of diffusion anisotropy. *Magn. Reson. Med.* 36, 893–906.
- Prayer, D., Roberts, T., Barkovich, A.J., Prayer, L., Kucharczyk, J., Moseley, M., Arieff, A., 1997. Diffusion-weighted MRI of myelination in the rat brain following treatment with gonadal hormones. *Neuroradiology* 39, 320–325.
- Privat, A., Jacque, C., Bourre, J.M., Dupouey, P., Baumann, N., 1979. Absence of the major dense line in myelin of the mutant mouse “shiverer”. *Neurosci. Lett.* 12, 107–112.
- Renfranz, P.J., Cunningham, M.G., McKay, R.D., 1991. Region-specific differentiation of the hippocampal stem cell line HiB5 upon implantation into the developing mammalian brain. *Cell* 66, 713–729.
- Segebarth, C., Belle, V., Delon, C., Massarelli, R., Decety, J., Le Bas, J.-F., Decroix, M., Benabid, A.L., 1994. Functional MRI of the human brain: predominance of signals from extracerebral veins. *NeuroReport* 5, 813–816.
- Seo, Y., Shinar, H., Morita, Y., Navon, G., 1999. Anisotropic and restricted diffusion of water in the sciatic nerve: a (^2H) double-quantum-filtered NMR study. *Magn. Reson. Med.* 42, 461–466.
- Shen, X.Y., Billings-Gagliardi, S., Sidman, R.L., Wolf, M.K., 1985. Myelin deficient (shimld) mutant allele: morphological comparison with shiverer (shi) allele on a B6C3 mouse stock. *Brain Res.* 360, 235–247.
- Song, S.K., Sun, S.W., Ramsbottom, M.J., Chang, C., Russell, J., Cross, A.H., 2002. Dysmyelination revealed through MRI as increased radial (but unchanged axial) diffusion of water. *Neuroimage* 17, 1429–1436.
- Stanisz, G.J., Webb, S., Munro, C.A., Pun, T., Midha, R., 2004. MR properties of excised neural tissue following experimentally induced inflammation. *Magn. Reson. Med.* 51, 473–479.
- Sukama, H., Nomura, Y., Takeda, K., Nakagawa, T., Tamagawa, Y., Ishii, Y., Tsukamoto, T., 1991. Adult and neonatal human brain: diffusional anisotropy and myelination with diffusion weighted MR imaging. *Radiology* 180, 229–233.
- Ulug, A.M., van Zijl, P.C., 1999. Orientation-independent diffusion imaging without tensor diagonalization: anisotropy definitions based on physical attributes of the diffusion ellipsoid. *J. Magn. Reson. Imaging* 9, 804–813.
- van den Pol, A.N., Ghosh, P.K., 1998. Selective neuronal expression of green fluorescent protein with cytomegalovirus promoter reveals entire neuronal arbor in transgenic mice. *J. Neurosci.* 18, 10640–10651.
- Wimberger, D.M., Roberts, T.P., Barkovich, A.J., Prayer, L.M., Moseley, M.E., Kucharczyk, J., 1995. Identification of “premyelination” by diffusion-weighted MRI. *J. Comput. Assist. Tomogr.* 19, 28–33.
- Xue, R., van Zijl, P.C., Crain, B.J., Solaiyappan, M., Mori, S., 1999. In vivo three-dimensional reconstruction of rat brain axonal projections by diffusion tensor imaging. *Magn. Reson. Med.* 42, 1123–1127.
- Zhang, J., van Zijl, P.C., Mori, S., 2002. Three-dimensional diffusion tensor magnetic resonance microimaging of adult mouse brain and hippocampus. *Neuroimage* 15, 892–901.